Available online at www.sciencedirect.com
SCIENCE DIRECT®
Optics Communications 253 (2005) 205–213
OPTICS COMMUNICATIONS
www.elsevier.com/locate/optcom

Application of RZ-scan technique for investigation of nonlinear refraction of sapphire doped with Ag, Cu, and Au nanoparticles

R.A. Ganeev [a,b,*], A.I. Ryasnyansky [c,d], A.L. Stepanov [e,f], C. Marques [g,h], R.C. da Silva [g,h], E. Alves [g,h]

[a] NPO Akadempribor, Academy of Sciences of Uzbekistan, Akademgorodok, Tashkent 700125, Uzbekistan
[b] The Institute for Solid State Physics, The University of Tokyo, 5-1-5 Kashiwanoha, Kashiwa, Chiba 277-8581, Japan
[c] Samarkand State University, Samarkand 703004, Uzbekistan
[d] Institut des Nano-Sciences de Paris, CNRS – Université Pierre et Marie Curie, Case 80, 140 rue de Lourmel, F75015 Paris, France
[e] Kazan Physics-Technical Institute, Russian Academy of Sciences, 420029 Kazan, Russian Federation
[f] Institute of Physics and Erwin Schrödinger Institute for Nanoscale Research, Karl-Franzens-University Graz, A-8010 Graz, Austria
[g] Dep. Física, ITN, E.N. 10, 2695-953 Sacavém, Portugal
[h] CFNUL, Av. Prof. Gama Pinto 2, 1649-003 Lisboa, Portugal

Received 14 October 2004; received in revised form 17 March 2005; accepted 25 April 2005

Abstract

The results of investigation of the nonlinear refraction of sapphire doped by Ag, Cu, and Au nanoparticles using the reflection Z-scan technique are presented. The real parts of the third-order nonlinear susceptibility of Ag:Al_2O_3, Au:Al_2O_3, and Cu:Al_2O_3 were measured using the fundamental wavelength of Nd:YAG laser radiation ($\lambda = 1064$ nm, $t = 55$ps). It was shown that the Ag:Al_2O_3 possessed by self-focusing properties ($n_2 = 1.8 \times 10^{-11}$ cm^2 W^{-1}), whereas the Au:Al_2O_3 and Cu:Al_2O_3 showed the self-defocusing properties ($n_2 = -1.46 \times 10^{-10}$ and -1.7×10^{-11} cm^2 W^{-1}, respectively). The real part of third-order nonlinear susceptibility of Au:Al_2O_3 was measured to be 10^{-8} esu. The mechanisms of nonlinear refraction are discussed.

PACS: 42.65.An; 42.65.Jx; 78.40.Kc; 78.67.Bf

Keywords: Metal nanoparticles; Nonlinear refraction; Reflection Z-scan

* Corresponding author. Tel.: +81 471 363367; fax: +81 471 363366.
E-mail address: r_ganeev@issp.u-tokyo.ac.jp (R.A. Ganeev).

0030-4018/$ - see front matter © 2005 Elsevier B.V. All rights reserved.
doi:10.1016/j.optcom.2005.04.061

1. Introduction

The high values of third-order nonlinear susceptibility ($\chi^{(3)}$) [1–4] and fast response [1,5,6] have drawn an interest on composite materials, in particular glass materials doped with metal nanoparticles. In order to achieve the high value of $\chi^{(3)}$ one can use the resonant peculiarities of investigated materials, in particular surface plasmon resonance (SPR) of metal nanoparticles. The investigations of $\chi^{(3)}$ in the vicinity of the SPRs of metals doped in various matrices were carried out in [1–5], and the values as high as $\chi^{(3)} = 1.2 \times 10^{-6}$ esu were reported for Au:Al_2O_3 at the wavelength of 532 nm [3]. The value of $\chi^{(3)}$ for Ag nanoparticles doped in glass matrices at the wavelength of the second harmonic radiation of Ti:sapphire laser ($\lambda = 400$ nm) was measured to be 1.5×10^{-7} esu [4]. At the same time, for the application of such materials one should know their nonlinear optical characteristics at the lasing wavelengths of commercial lasers (Nd:YAG (1064 nm), Ti:sapphire (800 nm), etc.).

There are different approaches for the investigation of nonlinear optical parameters of materials (degenerate four-wave mixing [7], nonlinear interferometry [8], Z-scan [9]). The latter technique allows determining both the value and the sign of nonlinear optical parameters (nonlinear refractive index n_2 and nonlinear absorption coefficient). There are several modifications of the Z-scan technique, such as transmission Z-scan (TZ-scan) [9], eclipsing Z-scan [10], reflection Z-scan (RZ-scan) [11,12], time-resolved Z-scan [13], etc. The RZ-scan has an advantage with comparing to the others that allows investigating the optical nonlinearities of samples possessing by limited transparency. This technique is based on the studies of the surface properties of materials, whereas the others are used for the investigation of bulk characteristics of media. The application of RZ-scan is presented in [14], where the nonlinear refraction was investigated in GaAs crystal at the wavelength of 532 nm at which this semiconductor is fully opaque. On the other hand, this technique can also be applied for transparent materials and can be used for the comparison with conventional TZ-scan.

We applied the RZ-scan for the investigation of nonlinear refraction of copper-, silver-, and gold-doped sapphire samples polished from one side and characterized by limited transparency using the laser radiation located far from the SPRs of these metals ($\lambda = 1064$ nm).

2. Experimental apparatus

Fig. 1 presents the experimental set-up of the RZ-scan measurements of nonlinear refraction. We used the Nd:YAG laser ($\lambda = 1064$ nm, $t = 55$ ps) operated at a 2-Hz pulse repetition rate. Laser radiation was focused by a 25-cm focal length lens (1). The maximum intensity and the beam waist radius in the focal plane were measured to be $I_0 = 7 \times 10^9$ W cm^{-2} and 72 μm, respectively. The investigated sample (2) was fixed on the translation table (11) and moved along the Z-axis. The angle of incidence of laser radiation on the surface of sample was 30°. A part of radiation was reflected from the beam splitter (10) and measured by photo-diode (3) to control the energy of laser pulses. The radiation reflected from the surface of sample was directed to the mirror (7) and than collected by the lens (8) that allowed registering all the reflected radiation by photo-diode (5). To decrease the influence of the instability of laser radiation, the ratio $R(z)$ between the reflected signal and the incident one was calculated.

In the case of RZ-scan the refractive nonlinearities are measured without aperture (for example, see [14]). In RZ-scan scheme, the phase changes

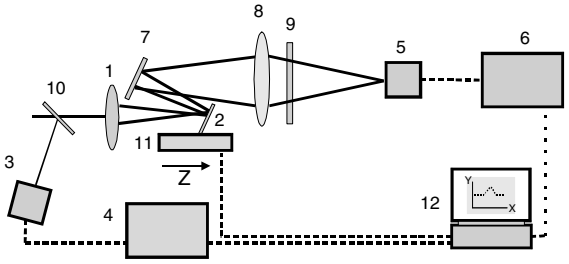

Fig. 1. Experimental set-up. 1: focusing lens; 2: investigated sample; 3,5: photo-diodes; 4,6: voltage converters; 7: mirror; 8: collecting lens; 9: neutral filters; 10: beam splitter; 11: translation table; 12: computer.

are produced by absorptive nonlinearities and the aperture is needed in this case. The refractive nonlinearities are responsible for the amplitude changes of reflected radiation so there is no need to use an aperture before the detector. The measurements of the refractive nonlinearities of samples (that are the subject of our studies) were carried out without an aperture, thus neglecting the influence of phase changes caused by nonlinear absorption. A behavior of normalized reflection Z-scans presented in Figs. 3, 5, and 7 indicates a nonlinear refraction phenomenon.

The principles of RZ-scan can be described as follows. The sample moves during the experiment through the focal plane of focusing lens. The amplitude and phase of reflected beam change due to the influence of nonlinear refraction and nonlinear absorption. No nonlinear effects appear when the sample is positioned far from the focal plane, so the ratio R of the reflected and incident laser radiation is constant. When the sample approaches focal plane, the laser intensity becomes higher and the nonlinear effects occur. In the case of positive nonlinear refraction ($n_2 > 0$), the movement of sample close to the focus leads to the growth of R. After crossing the focal plane the nonlinear refraction diminishes that leads to a decrease of R down to previous value. In the case of self-defocusing ($n_2 < 0$) the opposite feature will be observed with the valley appearing in the $R(z)$ dependence. One can conclude about the sign of n_2 from the $R(z)$ dependence.

We analysed the variations of reflected beam for the determination of the nonlinear refractive properties of our samples using the RZ-scans. The normalized reflected power could be presented as follows [14]:

$$P(z) = 1 + 2\mathrm{Re}\left[R(n_2 + \mathrm{i}k_2)\right]\frac{\int_0^\infty |E(\rho,z)|^4 \rho \mathrm{d}\rho}{\int_0^\infty |E(\rho,z)|^2 \rho \mathrm{d}\rho}, \quad (1)$$

where ρ and z are the radial and axial coordinates, k_2 is the nonlinear extinction coefficient, R is the relative change in the reflection coefficient, and $E(\rho, z)$ is the incident beam amplitude.

This equation describes the general case, when both nonlinear refraction and nonlinear absorption appear simultaneously during the reflection from the sample. However, the application of open-aperture RZ-scan allowed neglecting the influence of nonlinear absorption for the measurements of nonlinear refraction [15].

The artificial sapphire plates ($10 \times 10 \times 1$ mm) were unpolished from one side. The ion implantation was carried out by Ag^+, Cu^+ and Au^+ ions on the polished side of plates. The parameters of implantation and corresponding numbers of the samples are presented in Table 1. The detailed description of the synthesis of metal nanoparticles in dielectrics using the ion implantation was published elsewhere [16,17]. The optical properties of $Ag:Al_2O_3$, $Cu:Al_2O_3$ and $Au:Al_2O_3$ were analyzed by the reflection spectroscopy using two-beam spectrophotometer Perkin–Elmer Lambda 19.

Table 1
The preparation conditions for the synthesis of metal nanoparticles in Al_2O_3 and their nonlinear optical properties. I_0 is the laser radiation intensity in the focal plane, $\mathrm{Re}\,\chi^{(3)}$ is the real part of third-order nonlinear susceptibility

Sample	No.	Implantation energy, keV	Current density, μA/cm^2	Implantation dose, 10^{17} ion/cm^2	I_0, 10^9 W cm^{-2}	n_2, 10^{-11} cm^2 W^{-1}	$\mathrm{Re}\,\chi^{(3)}$, 10^{-9} esu
$Ag:Al_2O_3$	1	30	3	3.75	4.3	1.1	0.9
	2	30	6	3.75	4.3	1.3	1.1
	3	30	10	3.75	4.3	1.8	1.5
$Cu:Al_2O_3$	4	40	2.5	0.54	7.7	−1.3	−1.0
	5	40	12.5	1.00	7.7	−1.7	−1.4
$Au:Al_2O_3$	6	160	10	0.6	2.3	−9.4	−7.8
	7	160	10	0.6[a]	2.8	−12	−10
	8	160	10	1	2.3	−12.8	−11
	9	160	10	1[a]	1.8	−14.6	−12

[a] Thermal annealing.

The metal-containing sapphire is a very hard material and its preparation for TEM analysis is a complicated task. Because of this no TEM studies of metal-containing thin layers of sapphire can be found in literature. This is a rarely studied composite material, and that is why it is interesting to study a structure of nanoparticles in this matrix. In practice, it was possible observing nanoparticles structures in Au- and Cu-doped sapphires using atomic force microscope. From these studies we found that the implanted particles show a spherical shape, in agreement with a previous AFM study of Au nanoparticles created by ion implantation in sapphire [18]. At the same time, we analyzed the absorption spectra of these composite materials. The appearance of surface plasmon resonances in these spectra points out on the presence of metal nanoparticles. Using the Mie theory, we calculated the sizes of these particles and compared the experimental and theoretical spectra. Based on this analysis, the estimated sizes of nanoparticles in our samples were as follows: sample 1 – 10 nm, sample 2 – 15 nm, sample 3 – 20 nm, sample 4 – 10 nm, sample 5 – 15 nm, sample 6 – 5–8 nm, sample 7 – 10–15 nm, sample 8 – 10 nm, and sample 9 – 15–20 nm. The size distributions are likely to be quite broad based on the AFM measurements presented in [18].

Noting that the thermal annealing leads both to the appearance of additional Au nanoparticles and non-spherical particles that can cause an additional absorption in long-wavelength range.

Concerning the doses used in these studies, we noting that they were chosen to achieve the nanoparticles formation. In particular, the bombardment using high-energy (130 keV–2.1 MeV) copper ions did not lead to the nucleation of copper nanoparticles. So we used the implantation energy of 40 keV. The same can be said about other species.

3. Results

3.1. Ag:Al_2O_3

The linear reflection spectra of pure Al_2O_3 plate and three Ag:Al_2O_3 plates synthesized at different parameters of ion implantation are presented in Fig. 2. Samples 1–3 were implanted at the fixed dose (3.75×10^{17} ion/cm^2) and energy (30 keV) of ions, but using different values of current density of ionic beam. The thickness of a layer containing silver nanoparticles was 30 nm.

The implanted samples are characterized by a presence of broad selective lines of reflection in visible range that are associated with absorption in the range of 470 nm. The absorption of this band increased for the samples synthesized at high values of ionic current density. The appearance of absorption bands in the reflection spectra is an evidence of the formation of silver nanoparticles in Al_2O_3. This absorption band corresponds to the SPR of silver nanoparticles [16,17]. The sharp increase of the reflection in short-wavelength range (below 300 nm) was caused by the absorption of Al_2O_3 matrix and interband transitions of silver nanoparticles [19].

The growth of the current density of ionic beam at high implantation dose of silver ions in sapphire leads to the enhancement of SPR absorption. As the position of SPR maximum for all samples remains approximately the same, one can conclude that the growth of ionic current results in an increase of nanoparticles density, but not their size.

The $R(z)$ dependences for Ag:Al_2O_3 samples at $I_0 = 4.3 \times 10^9$ W cm^{-2} are shown in Fig. 3. One

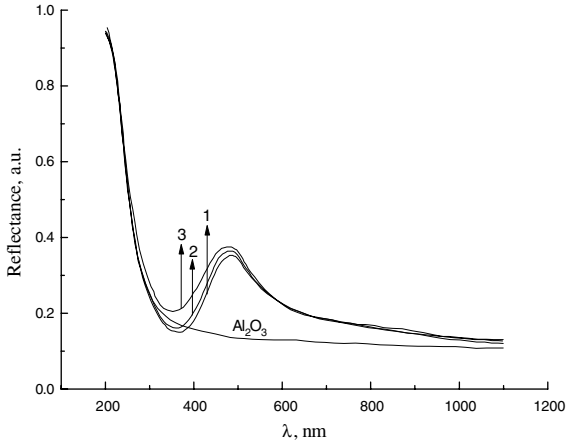

Fig. 2. The reflection spectra of pure Al_2O_3 and Ag:Al_2O_3 samples. The numbers in this and other figures correspond to the numbers of the samples.

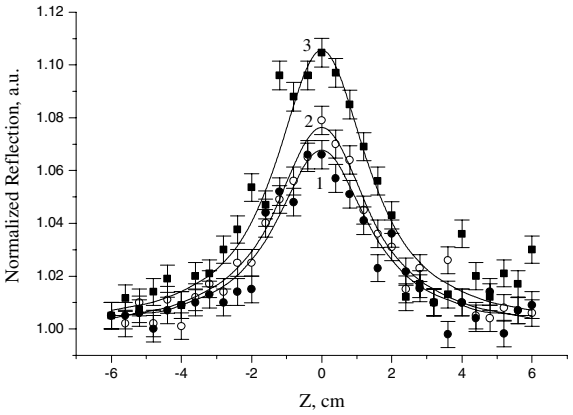

Fig. 3. The normalized reflection as a function of the position of Ag:Al_2O_3 samples. The solid lines in this and other figures show theoretical calculations.

can conclude from these dependences about the positive sign of nonlinear refraction for all samples. Note that the maximum of $R(z)$ dependence is higher for the samples implanted at higher ionic current density. The same experiments were carried out for pure Al_2O_3 and no changes of the normalized reflection were observed until the optical breakdown.

The simulations and fitting of $R(z)$ dependences were carried out using Eq. (1). The fitting of these dependences and experimental results allowed calculating the values of n_2 and $\mathrm{Re}\,\chi^{(3)}$ for samples 1, 2, and 3. The fitted dependences are presented in Fig. 3 as well as in other figures by solid lines and the values of optical nonlinearities are collected in Table 1.

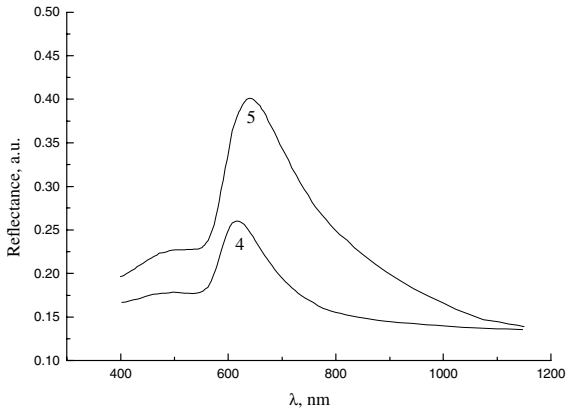

Fig. 4. The reflection spectra of Cu:Al_2O_3.

3.2. Cu:Al_2O_3

Samples 4 and 5 were produced by the ion implantation of copper ions in sapphire (sample 4: implantation dose 0.54×10^{17} ion/cm^2, ion current 2.5 μA/cm^2, and sample 5: implantation dose 10^{17} ion/cm^2, ion current 12.5 μA/cm^2). The energy of implantation in both cases was 40 keV. The thickness of the layer containing copper nanoparticles on the surface of Al_2O_3 was 40 nm [20].

The linear reflection spectra of samples 4 and 5 are presented in Fig. 4. The absorption bands were corresponded to the SPR of copper nanoparticles. The difference in position of the SPR of copper nanoparticles was discussed in [21] and can be explained by the presence of larger nanoparticles in sample 5 in comparison with sample 4.

The experimental and fitted $R(z)$ dependences for Cu:Al_2O_3 samples are presented in Fig. 5. A decrease of reflectivity of copper-containing samples approaching to the focus was caused by the self-defocusing of laser radiation. Note that the same difference in the signs of nonlinear refractive indices of Cu:Al_2O_3 and Ag:Al_2O_3 was previously observed for copper and silver nanoparticles doped in SiO_2 at the wavelength of 1064 nm [22]. The calculated values of n_2 and $\mathrm{Re}\,\chi^{(3)}$ of Cu:Al_2O_3 samples are presented in Table 1.

3.3. Au:Al_2O_3

In the case of gold-containing samples, we used two different doses (0.6×10^{17} and 10^{17} ion/cm^2) as well as in the case of Cu:Al_2O_3, however, the implantation was carried out at considerably higher energy (160 keV). The accumulation of implanted impurities in that case created a layer possessing by higher density of nanoparticles in comparison with low-energy implantation [23]. The implantation was carried out at high ionic current (10 μA/cm^2) to increase the mobility of implanted ions and stimulate nanoparticle nucleation. The thickness of a layer containing gold nanoparticles was 30 nm. In order to increase the sizes of nanoparticles, some of gold-coating

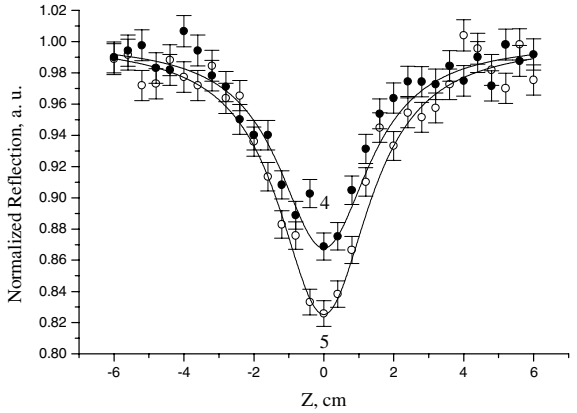

Fig. 5. The normalized reflection as a function of the position of Cu:Al_2O_3 samples.

samples were treated by a thermal annealing in oven during 1 h at 800 °C. The preparation conditions of Au:Al_2O_3 samples treated with (Nos. 7 and 9) and without (Nos. 6 and 8) thermal annealing are presented in Table 1.

The optical reflection spectra of Au:Al_2O_3 samples are shown in Fig. 6. The presence of gold nanoparticles was confirmed by the appearance of SPR spectral band near 610 nm. The appearance of wide reflection shoulder (sample 9), or even additional maximum (sample 7) can be caused by the re-distribution of metallic phase in dielectric volume after thermal annealing resulting in a formation of metal aggregates. The same

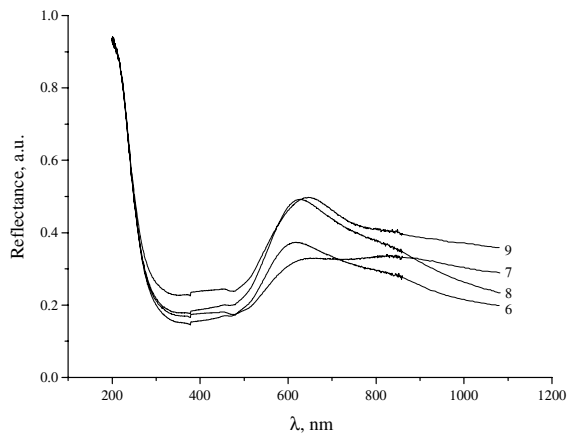

Fig. 6. The reflection spectra of Au:Al_2O_3 samples 6–9.

results have been previously observed in the case of silver colloids [24].

There are no reported studies, to the best of our knowledge, on the nonlinear optical properties of gold nanoparticles implanted in solid matrices and measured in near-infrared range (1064 nm). The results of our studies of nonlinear optical parameters of Au:Al_2O_3 samples are presented in Fig. 7. The observed $R(z)$ dependences show self-defocusing properties for all gold-containing samples. The data on n_2 and $\mathrm{Re}\,\chi^{(3)}$ of these samples are presented in Table 1.

4. Discussion

The possibility of the modification of metal nanoparticles-containing samples under the action of laser radiation during Z-scan studies was analysed in [25,26]. In our case, the experimental dependences showed a good reproducibility that is a confirmation that no structural modifications of samples occurred during experiments.

We analyzed the influence of thermal effect on observed nonlinear refraction. The appearance of thermal lens can be due to (“fast”) acoustic density changes [27] and (“slow”) thermal accumulation effects caused by heat accumulation between pulses [28]. In former case, the nonlinear thermal effect is a result of acoustic wave propagation due to matter density changing after local heating. The rise time (τ_1) that is necessary for observing the density variation and further the refractive index change determines by a ratio of beam waist radius at focal point to sound velocity in the medium (V_s): $\tau_1 = w_o/V_s$. Taking into account our experimental conditions, a rise time can be estimated as $\tau_1 \sim 80$ ns. Qualitatively, the former process can be explained by the consideration of individual picosecond pulse entering the medium and absorbing due to different mechanisms of absorption. Another process involved in this case is the thermal accumulation due to linear and/or nonlinear absorption. The time required for thermal conduction effects to become significant defines as $\tau_2 = w_o^2\rho' c_p/4\kappa$ [8], where c_p is the specific heat, ρ' is the density, and κ is the thermal conductivity. For our experimental conditions $\tau_2 \approx 1$ ms.

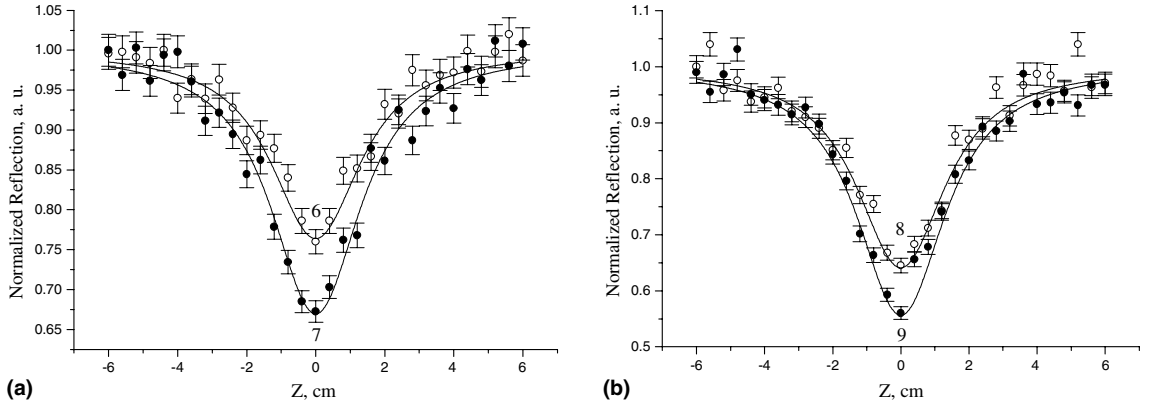

Fig. 7. The normalized reflections as functions of the position of Au:Al_2O_3 samples (a) 6 and 7, and (b) 8 and 9.

For the thermal effect to be important, it is necessary that the material possessed by high linear and/or nonlinear absorption. Another requirements are the, respectively, long pulse duration of probe radiation and/or high pulse repetition rate. The wavelength of used laser radiation was 1064 nm, which is far from the SPR and interband transitions, and the linear absorption was estimated to be in the range of 5%. We could not measure the transmittance of our samples because they were unpolished from one side. This estimation (5%) was taken from the measurements of analogous transparent glass samples doped with metals at the same concentration. The pulse duration was 55 ps, which is over than three orders of magnitude shorter than the time necessary for the propagation of acoustic wave through the focal area (80 ns). Finally, our laser operated at a 2-Hz pulse repetition rate, while for the appearance of thermal lens it is necessary to operate at the pulse repetition rate of the order of tens megahertz [28,29]. From above comments, we could assume that the thermal effects did not play important role in our experiments.

Our measurements have shown relatively high value of the real part of third-order nonlinear susceptibility ($\sim 10^{-8}$ esu) in the case of gold-implanted sapphire measured in near-infrared range, far from resonance lines. There were no changes in the normalized reflection of pure Al_2O_3 up to the maximum intensities used in these experiments ($I_0 = 7.7 \times 10^9$ W cm^{-2}), therefore, the observed nonlinear refraction was caused by metal nanoparticles. Previously reported value of n_2 for pure Al_2O_3 was 3×10^{-15} cm^2 W^{-1} [30] that is more than four orders of magnitude smaller than the values of n_2 of metal-implanted sapphire layer measured in our studies ($n_2 = 1.8 \times 10^{-11}$ cm^2 W^{-1} for Ag:Al_2O_3, $n_2 = -1.46 \times 10^{-10}$ for Au:Al_2O_3, and $n_2 = -1.7 \times 10^{-11}$ cm^2 W^{-1} for Cu:Al_2O_3 samples).

Optical Kerr effect (in the case of picosecond and femtosecond pulses) and thermal effect (in the case of nanosecond pulses) are the dominant processes responsible for the nonlinear refraction in such structures. The value of n_2 strongly depends on the type of laser interaction with medium (resonant or non-resonant). Note that non-resonant contributions to the refractive index are mostly positive [31].

The sign of n_2 in such composite structures is determined by a relation between fundamental (ω_{10}), or two-photon (ω_{20}) frequencies of laser radiation and any frequency of the resonances that may be presented (in the case of metal nanoparticles it is a SPR frequency ω_p). If one assumes that two-photon transitions are enhanced in the vicinity of the SPR, then there could be resonant contributions to n_2 that involve $\omega_{20} = 2\omega_{10}$. One can apply the relation for n_2 containing some terms that can considerably enhance a nonlinear refraction in the vicinity of resonance lines [32],

$$n_2(\omega_{10}) \propto \frac{A}{(\omega_p - \omega_{10})(\omega_p - \omega_{20})}, \tag{2}$$

where A is the independent constant.

In the used model, we considered not the atomic levels but the surface plasmon resonance and analyzed the frequency detuning of laser radiation from SPR of metal nanoparticles. Since the laser radiation frequency is far from the resonances in metal nanoparticles we took into account the possibility of two-photon process (for copper and gold). Note a good correlation between the signs of nonlinear refractive indices obtained experimentally and theoretically both in these and other studies of metal nanoparticles embedded in dielectric matrices [33,34]. However, the application of such a model should be analyzed further to confirm a connection with microscopic mechanisms that define the sign of the n_2 of our nanocomposites.

The values of ω_p of investigated metal-doped sapphires are in the range of 21,276 cm^{-1} (Ag, $\lambda_p \approx 470$ nm), 15,384–16,393 cm^{-1} (Cu, $\lambda_p \approx$ 610–650 nm), and 16,129–16,393 cm^{-1} (Au, $\lambda_p \approx 610$–620 nm). In the case, when the single-photon process is considered as a dominant one in laser–matter interaction ($\omega_{10} = 9398$ cm^{-1}, $\lambda = 1064$ nm) one can obtain from Eq. (2) the positive sign of n_2 for all the samples. This result coincides with our data for silver-containing sapphire, but contradicts our observations of self-defocusing properties in the cases of Cu- and Au-containing Al_2O_3. Taking into consideration the two-photon interaction of laser radiation ($\omega_{20} = 18{,}797$ cm^{-1}, $\lambda = 532$ nm) one can get from Eq. (2) the negative sign of n_2 for Au:Al_2O_3 and Cu:Al_2O_3, while the sign of n_2 for Ag:Al_2O_3 remains the same as in previous consideration ($n_2 > 0$), both results in good agreement with our measurements (see Table 2). The inclusion of two-photon process in the consideration of nonlinear refractive properties of our samples seems reasonable since the frequency of two photons of laser radiation is closer to the SPRs of investigated samples comparing to the fundamental frequency.

5. Conclusion

The RZ-scan technique was applied for the investigation of the nonlinear optical refraction of metal nanoparticles-containing sapphire samples characterized by limited transparency caused by unpolished back surface. The values of n_2 for silver-, copper- and gold-containing sapphire samples were determined (1.8×10^{-11} $cm^2\,W^{-1}$ for Ag:Al_2O_3, -1.46×10^{-10} $cm^2\,W^{-1}$ for Au:Al_2O_3, and -1.7×10^{-11} $cm^2\,W^{-1}$ for Cu:Al_2O_3). The signs of nonlinear refractive indices of these samples coincide with the estimations of the model taking into account the prevailing influence of two-photon processes on self-interaction properties of media.

Table 2
The signs of frequency detuning taking into account the single- and two-photon processes in different metal-containing samples and their nonlinear refractive indices

Sample	Δ_{10}	n_2^{theor}	Δ_{20}	n_2^{theor}	n_2^{exp}
Ag:Al_2O_3	+	+	+	+	+
Cu:Al_2O_3	+	+	–	–	–
Au:Al_2O_3	+	+	–	–	–

n_2 was estimated from Eq. (2); $\Delta_{10} = \omega_p - \omega_{10}$; $\Delta_{20} = \omega_p - \omega_{20}$.

The growth of ionic current stimulated the mobility of implanted ions and nanoparticles nucleation. The last process also led to the growth of the nonlinear refraction of samples. Our measurements showed high value of the real part of third-order nonlinear susceptibility in the case of gold-implanted sapphire in the near infrared range ($\sim 10^{-8}$ esu).

Acknowledgements

The authors thank Prof. T. Usmanov for providing the laser equipment for Z-scan measurements.

References

[1] R.F. Haglund, L. Yang, R.F. Magruder, J.E. Wittig, K. Becker, R.A. Zuhr, Opt. Lett. 18 (1993) 373.
[2] J. Olivares, J. Requejo-Isidro, R. Del Coso, R. De Nalda, J. Solis, C.N. Afonso, A.L. Stepanov, D. Hole, P.D. Townsend, A. Naudon, J. Appl. Phys. 90 (2001) 1064.
[3] H.B. Liao, R.F. Xiao, J.S. Fu, K.G.L. Wong, Appl. Phys. B 65 (1997) 673.
[4] H. Inouye, K. Tanaka, I. Tanahashi, T. Hattori, H. Nakatsuka, Jpn. J. Appl. Phys. 39 (2000) 5132.

[5] N. Kashimoto, Y. Takeda, N. Umeda, N. Okubo, R.G. Faulkner, Nucl. Instr. Meth. B 206 (2004) 634.
[6] M. Lee, T.S. Kim, Y.S. Choi, J. Non. Cryst. Solids 211 (1997) 143.
[7] S.R. Friberg, P.W. Smith, IEEE J. Quantum Electron. 23 (1987) 2089.
[8] M.J. Morgan, C.Y. She, R.L. Carman, IEEE J. Quantum Electron. 11 (1975) 259.
[9] M. Sheik-Bahae, A.A. Said, T.-H. Wei, D.J. Hagan, E.W. Van Stryland, IEEE J. Quantum Electron. 26 (1990) 760.
[10] T. Xia, D.J. Hagan, M. Sheik-Bahae, E.W. Van Stryland, Opt. Lett. 19 (1994) 317.
[11] D.V. Petrov, A.S.L. Gomes, C.B. de Araujo, Appl. Phys. Lett. 65 (1994) 1067.
[12] D.V. Petrov, A.S.L. Gomes, C.B. de Araujo, Opt. Commun. 123 (1996) 637.
[13] T. Kawazoe, H. Kawaguchi, J. Inoue, O. Haba, M. Ueda, Opt. Commun. 160 (1999) 125.
[14] M. Martinelli, L. Gomes, R.J. Harowicz, Appl. Opt. 39 (2000) 6193.
[15] R.A. Ganeev, A.I. Ryasnyansky, Phys. Stat. Sol. (a) 202 (2005) 120.
[16] A.L. Stepanov, D.E. Hole, Recent Res. Devel. Appl. Phys. 5 (2002) 1.
[17] A.L. Stepanov, Rev. Adv. Mater. Sci. 4 (2003) 45.
[18] D.O. Henderson, R. Mu, Y.S. Tung, M.A. George, A. Burger, S.H. Morgan, C.W. White, R.A. Zuhr, R.H. Magruder, J. Vac. Sci. Technol. B 13 (1995) 1198.
[19] U. Kreibig, M. Vollmer, Optical Properties of Metal Clusters, Springer, Berlin, 1995.
[20] A.L. Stepanov, Tech. Phys. Lett. 28 (2003) 58.
[21] A.L. Stepanov, U. Kreibig, D.E. Hole, R.I. Khibullin, I.B. Khaibullin, V.N. Popok, Nucl. Instr. Meth. B 178 (2001) 20.
[22] R.A. Ganeev, A.I. Ryasnyansky, A.L. Stepanov, T. Usmanov, Phys. Stat. Sol. (b) 241 (2004) 935.
[23] A.L. Stepanov, V.A. Zhikharev, D.E. Hole, P.D. Townsend, I.B. Khaibullin, Nucl. Inst. Meth. B 166–167 (2000) 26.
[24] S.V. Karpov, V.V. Slabko, M.K. Kodirov, A.I. Ryasnyansky, Quantum Electron. 31 (2001) 904.
[25] R. Serna, J.M. Ballesteros, J. Solis, C.N. Afonso, D.H. Osborne, R.F. Haglung, A.K. Petford-Long, Thin Solid Films 318 (1998) 96.
[26] D.H. Osborne, R.F. Haglund, F. Gonella, F. Garrido, Appl. Phys. B 66 (1998) 517.
[27] H. Toda, C.M. Werber, Opt. Lett. 17 (1992) 1379.
[28] M. Falconieri, G. Salvetti, Appl. Phys. B 69 (1999) 133.
[29] S. Couris, M. Renard, O. Faucher, B. Lavorel, R. Chaux, E. Koudoumas, X. Michaut, Chem. Phys. Lett. 369 (2003) 318.
[30] R. Adair, L.L. Chase, S.A. Payne, Phys. Rev. B 39 (1989) 3337.
[31] A. Owyoung, IEEE J. Quantum Electron. 9 (1973) 1064.
[32] J.F. Reintjes, Nonlinear Optical Parametrical Processes in Liquids and Gases, Academic, Orlando, 1984.
[33] R.A. Ganeev, A.I. Ryasnyansky, A.L. Stepanov, T. Usmanov, Phys. Stat. Sol. (b) 238 (2003) R5.
[34] R.A. Ganeev, A.I. Ryasnyansky, A.L. Stepanov, T. Usmanov, Phys. Stat. Sol. (b) 241 (2004) 935.